UC Santa Barbara

Title

Hydrophobic, Electrostatic, and Dynamic Polymer Forces at Silicone Surfaces Modified with Long-Chain Bolaform Surfactants

Permalink

https://escholarship.org/uc/item/11c5p8qm

Authors

Rapp, MV
Donaldson, SH
Gebbie, MA
et al.

Publication Date

2015

DOI

10.1002/smll.201402229

Copyright Information

Peer reviewed

Hydrophobic, Electrostatic, and Dynamic Polymer Forces at Silicone Surfaces Modified with Long-Chain Bolaform Surfactants

Michael V. Rapp, Stephen H. Donaldson Jr., Matthew A. Gebbie, Saurabh Das, Yair Kaufman, Yonas Gizaw, Peter Koenig, Yuri Roiter, and Jacob N. Israelachvili*

Surfactant self-assembly on surfaces is an effective way to tailor the complex forces at and between hydrophobic-water interfaces. Here, the range of structures and forces that are possible at surfactant-adsorbed hydrophobic surfaces are demonstrated: certain long-chain bolaform surfactants—containing a polydimethylsiloxane (PDMS) mid-block domain and two cationic α, ω-quarternary ammonium end-groups—readily adsorb onto thin PDMS films and form dynamically fluctuating nanostructures. Through measurements with the surface forces apparatus (SFA), it is found that these soft protruding nanostructures display polymer-like exploration behavior at the PDMS surface and give rise to a long-ranged, temperature- and rate-dependent attractive bridging force (not due to viscous forces) on approach to a hydrophilic bare mica surface. Coulombic interactions between the cationic surfactant end-groups and negatively-charged mica result in a rate-dependent polymer bridging force during separation as the hydrophobic surfactant mid-blocks are pulled out from the PDMS interface, yielding strong adhesion energies. Thus, (i) the versatile array of surfactant structures that may form at hydrophobic surfaces is highlighted, (ii) the need to consider the interaction dynamics of such self-assembled polymer layers is emphasized, and (iii) it is shown that long-chain surfactants can promote robust adhesion in aqueous solutions.

M. V. Rapp, Dr. S. H. Donaldson Jr., S. Das,
Dr. Y. Kaufman, Prof. J. N. Israelachvili
Department of Chemical Engineering
University of California
Santa Barbara (UCSB), CA 93106-5080, USA
E-mail: jacob@engineering.ucsb.edu

M. A. Gebbie, Prof. J. N. Israelachvili
Materials Department
University of California, Santa Barbara (UCSB)
CA 93106-5050, USA

Dr. Y. Gizaw, Dr. Y. Roiter
The Procter & Gamble Co. Winton Hill Business Center
6210 Center Hill Avenue, Cincinnati, OH 45224, USA

Dr. P. Koenig
The Procter & Gamble Co.
Modeling and Simulation/Computational Chemistry
8611 Beckett Road, West Chester, OH 45069, USA

1. Introduction

Silicone products are ubiquitous in modern life, spanning from cosmetic products at home to designer surfaces in the laboratory. Boasting a favorable set of material properties—including hydrophobicity, biocompatibility, optical transparency, low chemical reactivity, low surface tension, and unique tribological properties—viscoelastic silicones are widely used in applications such as biomedical implants,[1,2] contact lenses,[3] scaffolds for tissue engineering,[4] and lubricating films.[5,6] Polydimethylsiloxane (PDMS) is the most commonly used silicone compound in research, industrial, and consumer product applications. In the lab, PDMS can be (i) molded into microfluidic channels for lab-on-a-chip diagnostic experiments,[7] (ii) patterned with lithography to form micron-scale surface features that control adhesion, friction, and wettability,[8,9] or (iii) functionalized and dispersed in water to form

stimuli-responsive hydrogels[10,11] and emulsions.[12] In consumer products such as fabric softeners and cosmetic creams, PDMS is used to form thin lubricating films that impart a favorable tactile sensation onto clothes or skin.[5,13]

In many of these practical applications, the desired functionality of the PDMS material—in situ wet adhesion, lubrication, or colloidal stabilization—is based upon the aqueous interfacial properties of either a plain or a functionalized PDMS surface. To understand the interfacial forces that exist at PDMS surfaces, a method to reliably prepare thin (6–10 nm), smooth (≈0.3 nm rms roughness), and covalently-grafted collapsed-brush PDMS films on extended gold or mica substrates was developed previously.[14] These PDMS films serve as nano-thin templates to explore the interfacial forces at plain or functionalized silicone surfaces. When exposed to water, the hydrophobic surface of PDMS dewets, and water forms large contact angles on the surface (advancing contact angle, $\theta_A = 113° \pm 2°$, and receding contact angle, $\theta_R = 103° \pm 2°$). Through measurements with the surface forces apparatus (SFA), the PDMS surface was found to display a negative surface charge in solution at pH > 3 (≈−100 ± 20 mV at pH 10 in 1 mM NaCl), a characteristic of most hydrophobic surfaces.[15–18] The interaction between the negatively charged PDMS surface and a negatively charged mica surface at pH 10 results in a monotonic repulsion between the surfaces that is due to the repulsive osmotic pressure between the surface's overlapping electric double layers at large distances (>≈1 Debye screening length) and due to the steric hydration forces between the surfaces at small separation distances (<≈2 nm).

The negative charge on the PDMS surface can be problematic for certain applications. In a wet environment, attractive van der Waals forces are not strong enough to overcome the repulsive electrostatic and hydration forces that exist between a PDMS surface and another negatively charged surface (such as a mineral, metal, cotton, or keratin). In applications that require strong binding of a PDMS interface to a negatively charged surface in solution—say, securing a prosthetic silicone implant onto bone, or binding lubricating thin films of silicone onto hair—PDMS surface functionalization is required for robust adhesion. The hydrophobicity of the PDMS surface can be exploited by adsorbing amphiphilic molecules onto the surface, leading to non-destructive physisorbed surface modifications that enhance the adhesive potential of PDMS. Amphiphilic polymers[19,20] and polyelectrolytes[21–23] are frequently adsorbed onto hydrophobic surfaces to reduce friction or wear at hydrophobic polymer surfaces. Intrinsically unstructured proteins extracted from the adhesive plaques of marine mussels adsorb to hydrophobic surfaces via hydrophobic amino acid residues, and mediate adhesion to a hydrophilic mineral surface.[24–26] Quaternary ammonium polyelectrolytes function as biofunctional coatings when adsorbed onto PDMS and facilitate the attachment and growth of bone marrow cells.[27] However, the physisorption of polymeric surfactants has not been explicitly used to promote adhesion between hydrophobic and hydrophilic surfaces.

The adsorption of adhesion-promoting amphiphiles or surfactants onto a hydrophobic surface is fundamentally interesting when considering the intermolecular forces that determine the equilibrium geometry of the surface aggregates. In bulk solution above the critical micelle concentration (CMC), the self-assembly of ionic surfactants depends on a balance of forces between the hydrophobic attractions between surfactant tails, the electrostatic repulsion between surfactant head-groups, and geometric packing constraints.[28] Comparatively, ionic surfactants self-assemble at hydrophobic surfaces above a critical aggregation concentration (CAC, where CAC < CMC). The balance of forces that govern surface assembly becomes more complex as additional parameters are introduced, namely the hydrophobic attraction between the surfactant tails and the surface, and the geometric constraints of the surface. Previous research has shown that short-chain aliphatic surfactants (cetyl trimethylammonium halides, sodium dodecyl sulfate, alkylpoly[ethylene oxide], C_{12} zwitterionic surfactants) adsorb onto solid hydrophobic surfaces (crystalline graphite, methylated silica) and may form a variety of aggregate morphologies (monolayers, flat discs, hemimicelles, hemicylinders) that are dependent upon surfactant geometry, headgroup type, the surfactant concentration, and the type of hydrophobic surface.[29–34] Force measurements with the atomic force microscope (AFM) indicate that these adsorbed ionic layers give rise to time-invariant and exponentially decaying double layer forces between an AFM probe and the surfactant-adsorbed substrate.[31,35] While there is undoubtedly a constant exchange of surfactant monomers between the surface aggregates and solution, the previous reports on these aggregates indicate that their shapes do not dynamically change or fluctuate in a significant way over the timescale of an AFM measurement (with typical AFM line scan rates of 0.1 to 1 µm s⁻¹). The static nature and relatively simple geometries of these surface aggregates perhaps are not surprising, as the majority of the studied surfactants adsorb from small spherical micelles in solution to form surface features that are similar in dimension to the size of their bulk micelles (≈2–5 nm). We hypothesize that increasing the complexity of the system—including adding long polymer chains and multiple headgroups to the adsorbing surfactants, altering the structure of the bulk surfactant aggregates, and using grafted chains of soft polymers as the hydrophobic surface—may result in more complex morphologies and dynamic (time-dependent) behaviors at self-assembled surfaces.

In this work, we investigate the self-assembly phenomenon of a long-chain bolaform surfactant as it adsorbs onto a grafted PDMS brush film. The bolaform surfactant (bolaquat-PDMS or bq-PDMS, **Figure 1**A) contains a linear PDMS mid-block domain and cationic α, ω-quarternary ammonium headgroups. As shown schematically in Figure 1B, bq-PDMS forms vesicles in solution; both cryogenic transmission electron microscopy (TEM) images (Figure 1C) and dynamic light scattering (DLS) confirmed that the vesicles are spherical with an average diameter of ≈100 nm. In the following experiments, we adsorbed vesicles of bq-PDMS onto gold-grafted PDMS brush films (Au-PDMS, Figure 1D) to obtain a bq-PDMS functionalized interface. Using the SFA, we measured the normal interaction forces in aqueous solution between (i) a negatively-charged mica surface and an
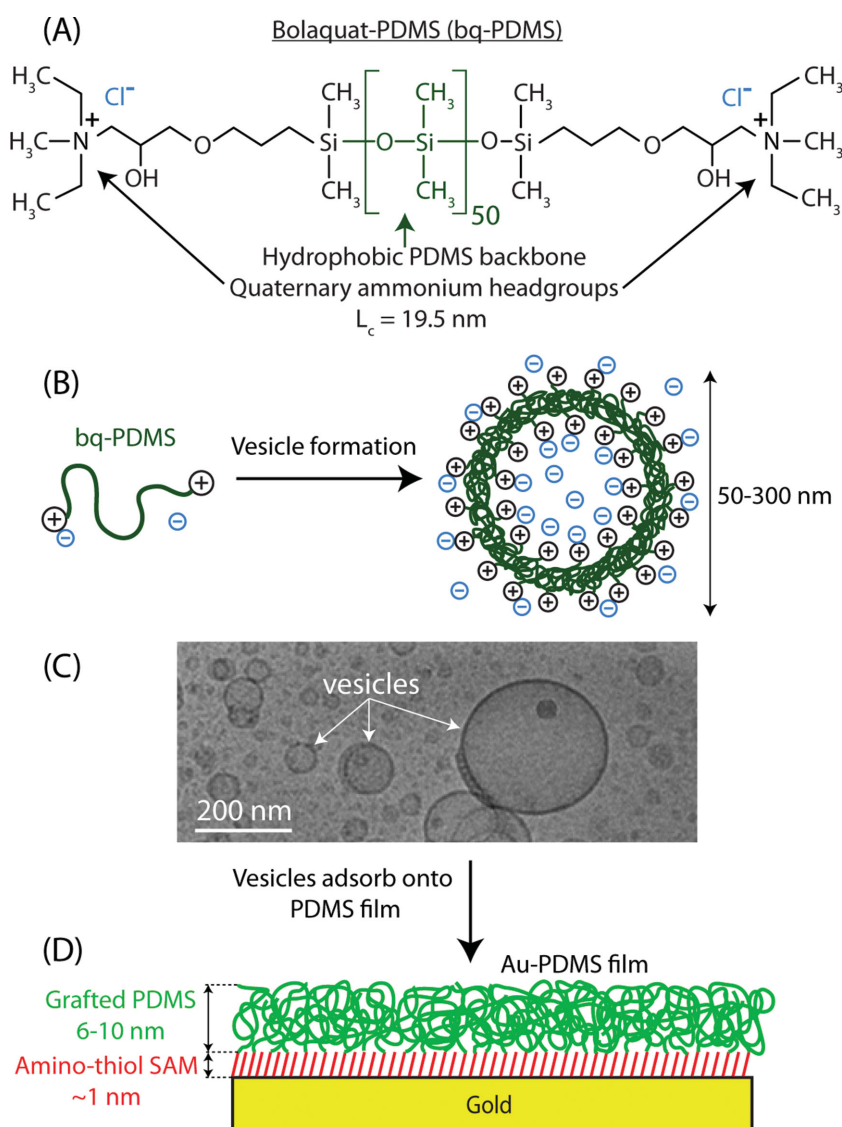
Figure 1. The long-chain bolaform surfactant and the grafted silicone surfaces used in this study. (A) The chemical structure of bolaquat-PDMS (bq-PDMS). (B) A schematic representation of bq-PDMS vesicles. (C) A representative cryo-TEM image of 1% v/v bq-PDMS dispersed in water. The bq-PDMS typically forms spherical single unilamellar vesicles from ≈50 nm up to ≈300 nm in diameter. Some small bq-PDMS aggregates (≈10–20 nm diameter) are also observed. (D) A schematic representation of the thin, covalently-grafted PDMS films on gold that are used in this study.

accuracy, visualization, and versatility for measuring force-distance curves between extended soft matter surfaces and structures.[36] The SFA utilizes a technique known as fringes of equal chromatic order (FECO), in which the wavelengths of light interference fringes are used to measure the absolute separation distance, D, between two extended cross-cylinder surfaces with an accuracy of ≈1 Å.[37] The radius of the macroscopic interacting surfaces, $R ≈ 2$ cm, is also measured by FECO. The interaction force between the two surfaces, F, is measured by the deflection of a double-cantilevered spring with a known spring constant, k. When measuring forces between attractive or adhesive surfaces, mechanical instabilities occur when the slope of the interaction force between the two surfaces equals the spring constant ($dF/dD = k$), and the surfaces rapidly jump into an adhesive contact on approach, or jump out of adhesive contact as the surfaces are separated. The FECO provide a real-time virtual image of the interacting surfaces during the force measurement, through which the separation distance (D), contact mechanics, adhesion, and deformations of the interacting surfaces can be determined. The SFA technique measures the absolute separation distance between the surfaces at all times, which allows for the accurate measurements of time-dependent forces (ranging from transient to long-equilibrating forces) that are frequently found in polymer or biological systems.

A typical force-distance curve plots the force scaled by radius (F/R) versus the surface separation distance (D). Typically, the force, F, is normalized by the radius, R, to allow for comparison with separate experiments and techniques because interaction forces scale with R. An advantage of the SFA—which is important especially for the interactions examined in this work—is the ability to explore a wide range of surface approach and separation rates, v, which ranges from $v ≈ 0.1$ to 10 nm s^{-1}. Two measurement techniques were used in the present study: (1) a "dynamic" technique and (2) a "quasi-static" technique. In a dynamic measurement, the surfaces are driven towards each other at a constant rate, $v ≈ 2$–10 nm s^{-1}, while measuring the force instantaneously at each separation distance in the force curve. In a quasi-static measurement, the equilibrium force between the surfaces is measured after the surfaces are equilibrated for 30 seconds at a given separation distance. The surfaces are then moved to a new separation distance (step size ≈ 5 nm) and allowed to equilibrate again for 30 s before measuring the equilibrium force ($v_{average} ≈ 0.2$ nm s^{-1}). The

adsorbed bq-PDMS film and (ii) two symmetric bq-PDMS films. The results show that bq-PDMS self-assembles into soft, fluctuating nanostructures on the grafted-PDMS surface that give rise to dynamic polymer bridging forces between extended surfaces. Furthermore, a sparingly low concentration of bq-PDMS mediates exceptionally strong adhesion between mineral (mica) and polymer (PDMS) surfaces.

2. Results and Discussion

The SFA was used in this work to examine the interaction forces primarily between a bq-PDMS functionalized surface and a mica surface. The SFA provides distinct advantages in

quasi-static technique provides the most accurate equilibrium force measurements and can detect forces that may take tens of seconds to equilibrate, such as polymer bridging forces.[38] In both dynamic and quasi-static SFA measurements, the approach and separation rates are so slow that hydrodynamic (viscous) forces between the surfaces are negligible, and the measured forces are incontrovertibly due to interaction of a bq-PDMS film with a mica surface. The differences between quasi-static and dynamic measurements, and their implications on the physical interactions and structures of bq-PDMS, will be discussed in detail below.

To determine the interactions of the bq-PDMS film with a mica surface, the bq-PDMS was initially adsorbed, via vesicles, onto an Au-PDMS grafted layer. This bq-PDMS-coated surface was then mounted in the SFA opposite a clean mica surface for the force measurement while immersed in 1 mM NaCl, pH ≈ 10 solution. As discussed below, the interactions during both approach and separation of the bq-PDMS at the target mica surface are strongly attractive. The approach and separation curves are both very complex and appear to be governed by somewhat different physical mechanisms, so we first discuss the approach in Section 2.1.

2.1. Asymmetric Interactions Between bq-PDMS and Mica Surfaces During Approach
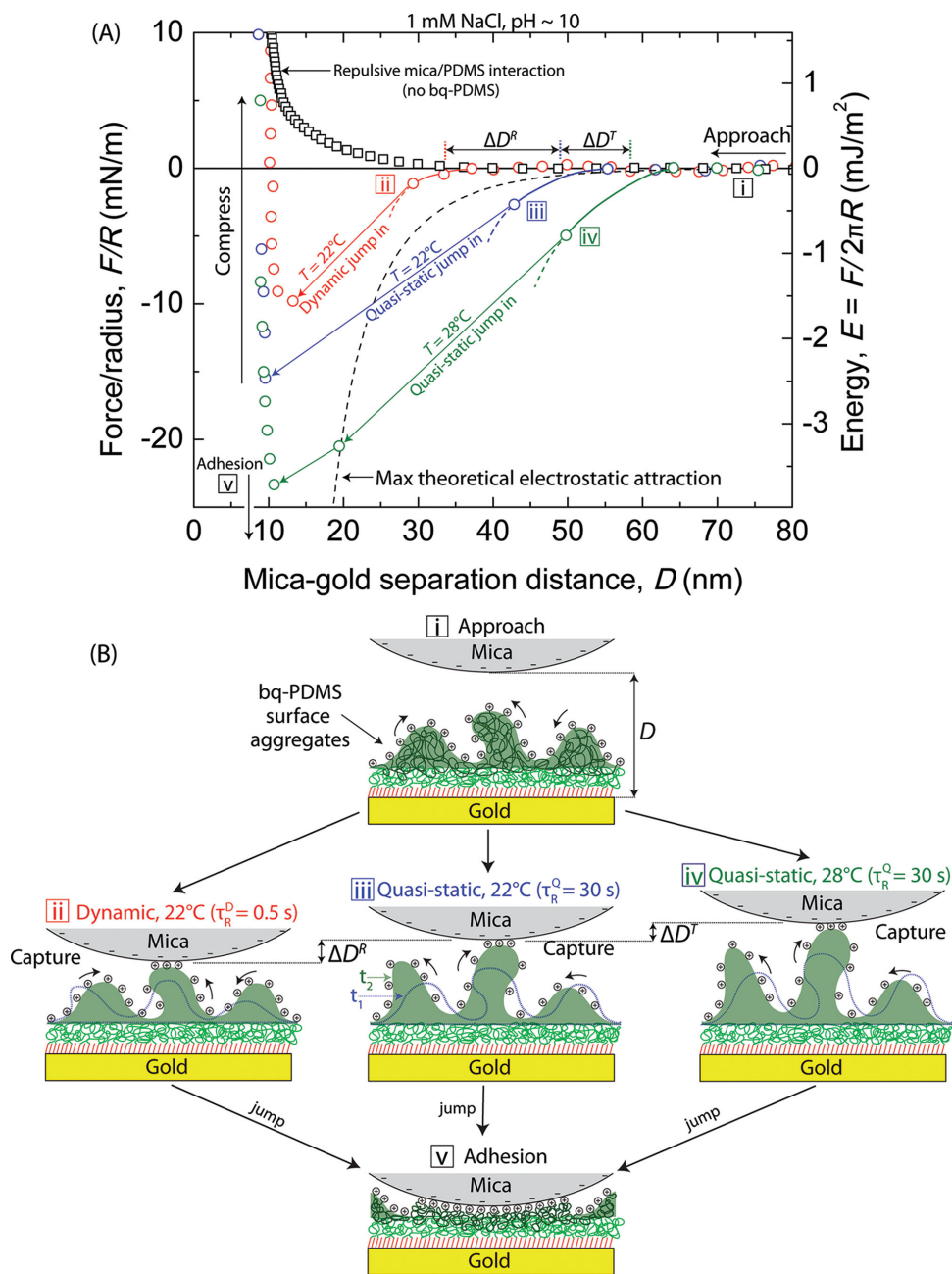
The interactions during approach of a bq-PDMS film and mica exhibit a long-range attractive jump-in to contact that depends sensitively on the rate of approach of the two surfaces, as shown in **Figure 2**A. At room temperature (T = 22 °C), when a bq-PDMS film and mica are driven towards each other at a rate $v \approx 6$ nm s^{-1} (dynamic), an attractive force is first measured at $D \approx 33$ nm, and is followed by a jump into adhesive contact to the contact distance, $D_0 = 10$ nm (red points, Figure 2A). When the surface approach is quasi-static, the onset of attraction increases dramatically to $D \approx 49$ nm, and the surfaces subsequently jump into contact from a much greater distance (blue points, Figure 2A). Raising the temperature, from room temperature to T = 28 °C, results in the onset of attraction increasing further, to $D \approx 58$ nm (green points, Figure 2A). For comparison, the interaction of a clean Au-PDMS surface (i.e., in the absence of bq-PDMS) with a mica surface is also shown (black points, Figure 2A). As described previously,[14] the interaction is fully repulsive (in 1 mM NaCl solution at pH ≈ 10). The maximum attractive electric double layer interaction between negatively charged mica and a fully-charged cationic surface (as might be expected for an adsorbed monolayer of bq-PDMS) is also shown for comparison (dashed black line, Figure 2A).

The measured attractive forces for both the room temperature and elevated temperature quasi-static measurements are much stronger and longer-ranged than the maximum electrostatic force, so a simple electrostatic double layer attraction between the cationic bq-PDMS and negatively-charged mica can be ruled out. The attraction is also longer-ranged than the fully extended length of the bq-PDMS molecule (contour length, $L_C \approx 20$ nm), indicating that a molecular extension event cannot explain the measured

attraction. Molecular bridging can be further ruled out because there would be a large energy penalty for extending the hydrophobic central block of the bq-PDMS molecules into the aqueous solution, which would be necessary for a molecular bridging between bq-PDMS headgroups and mica. Quasi-static SFA measurements between a bq-PDMS film and mica in 100 mM NaCl show a slightly shorter-ranged attraction and jump-in distance, but the interaction is still much stronger and longer-ranged than any expected electrostatic attraction between the oppositely charged interfaces (Supporting Information, Figure S1).

The rate dependence, temperature dependence, and ionic strength dependence of the bq-PDMS and mica SFA measurements lead to the hypothesis that nanoscale, micelle-like, and dynamically fluctuating aggregates of bq-PDMS protrude from the bq-PDMS/Au-PDMS interface, leading to the observed capture and subsequent strong adhesion between the two interacting surfaces (shown schematically in Figure 2B). These nanoscale aggregates likely behave similarly to grafted polymers or cylindrical micelles, with similar relaxation times and temperature effects, as they fluctuate near the PDMS surface due to constrained Brownian motion (Figure 2B.i). At the surface, the aggregates diffuse within a given configuration space and statistically explore all of their possible configurations. The onsets of the attractions in the measured force profiles correspond to rare events when an aggregate samples an extended configuration and binds to the approaching mica surface with the quaternary ammonium headgroups (referred to as "capture" events). At a fixed separation distance, the probability of a capture event increases with time. Accordingly, during a quasi-static approach (Figure 2B.iii), the longer equilibration time (30 s) at each separation distance results in a capture event that occurs at a much larger separation distance than when the approach is performed dynamically (0.5 s between each measurement point, Figure 2B.ii). The additional energy provided by increasing the temperature leads to an increase in the rate, size, and exploration space of the fluctuating bq-PDMS aggregates, leading to a greater onset of attraction at the elevated temperature (Figure 2B.iv). Quaternary ammonium groups are known to form a strong ionic bond with binding energy of ≈5–9 kT at mica surface sites in aqueous solution.[39,40] The specific Coulombic bond between the quaternary ammonium headgroups and the mica surface allows for the capture of the mica surface, while the hydrophobic interaction between the bq-PDMS surfactant chains and Au-PDMS chains leads to the ultimate collapse of the layer (Figure 2B.v).

The dynamics of the surface aggregates as they explore space and bind to the mica can be analyzed in terms of mean-field theories, similar to the scaling theories originally developed for end-grafted polymer chains by de Gennes.[41] As described by Wong *et al* for tethered ligand-receptor interactions,[42] in this case the analogous aggregates diffuse within a given configuration space, exploring all possible configurations, with the range of the attraction depending on the equilibration time at each separation distance. The typical time for an aggregate to sample a configuration at an extended distance, D_E, is known as the exploration time, τ_R, and is given by

Figure 2. The interactions of a mica surface approaching a film of adsorbed bq-PDMS. (A) Comparative SFA force-distance measurements of the interaction between mica and an adsorbed bq-PDMS film, performed either dynamically (red circles, approach speed of $v \approx 6$ nm s^{-1}) or quasi-statically (30 second equilibration periods were allowed after each approach step of ≈ 5 nm). Quasi-static measurements are shown for $T = 22$ °C (blue circles) and $T = 28$ °C (green circles). The solid colored lines (red, blue, green) show the probable interaction potentials for each measurement, and these curves continue as dashed colored lines in the unstable regions after the points where the surfaces abruptly jump into adhesive contact. The black dashed curve indicates the theoretical maximum attractive electrostatic double-layer force between a mica surface and a fully ionized cationic surface. The monotonically repulsive PDMS/mica interaction in the absence of adsorbed bq-PDMS is shown for reference (black squares). (B) Schematic representations of the hypothesized interacting structures. The images are intended as visual aids and are not drawn to scale. (i) The mica surface approaches the bq-PDMS film. The bq-PDMS 'micelle-like' aggregates contact the mica surface at a smaller separation distance when the approach is performed dynamically (ii) than if the approach is performed quasi-statically (iii). As the temperature is increased (iv), the bq-PDMS aggregates contact the mica surface at an even greater separation distance. In schematics (ii), (iii), and (iv), the blue dashed line indicates the outline of the bq-PDMS aggregates at an initial time t_1 and the green shaded region indicates the position of the aggregates when they contact (capture) the incoming mica surface at time t_2 ($t_2 > t_1$). (v) The mica surface jumps into a strong adhesive contact with the underlying PDMS layer.

$\tau_R(D_E) = \tau_0 \cdot \exp[E_{ext}(D_E)/k_B T]$, where $E_{ext}(D_E)$ is an external potential, τ_0 is the intrinsic relaxation rate of a single polymeric aggregate, k_B is Boltzmann's constant and T is the temperature. The intrinsic relaxation rate of a single aggregate is known as the Zimm time,[43] $\tau_0 \approx \eta R_F^3/k_B T$, where η is the viscosity of water, and R_F is the effective Flory radius of the polymer aggregate. The external potential can be approximated as a parabolic potential, $E_{ext}(D_E) = D_E^2 k_B T / 2R_F^2$,
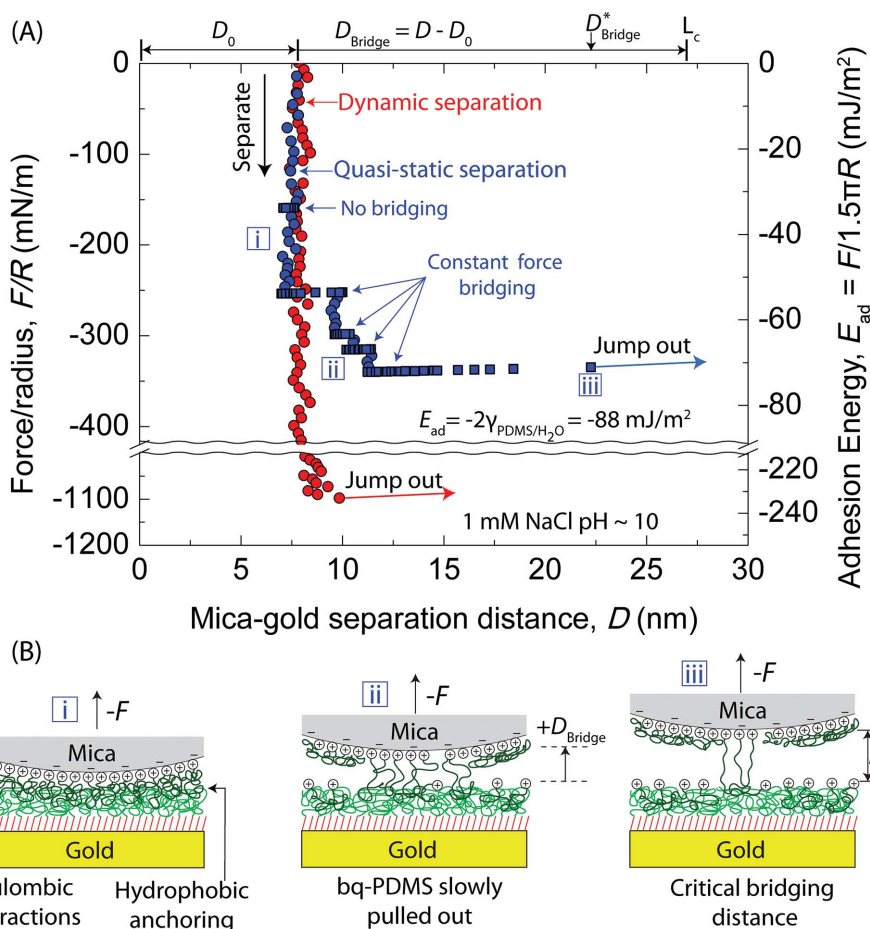
Figure 3. The adhesive interactions of a mica surface separating from a film of adsorbed bq-PDMS. (A) Dynamic (red circles) and quasi-static (blue circles/squares) force-distance measurements for the separation of a mica surface from the PDMS/bq-PDMS interface. At certain times during the quasi-static separation (marked with blue squares) the surfaces were allowed to fully equilibrate while under constant tensile load. In this particular quasi-static separation, constant force bridging between the surfaces is first observed at a tensile load of ≈−250 mN/m, as bq-PDMS molecules are pulled out from the grafted PDMS film. (B) A schematic representation of the interaction potential during the quasi-static separation of the surfaces. (i) Coulombic (headgroup-mica) interactions strongly bind the mica surface to the bq-PDMS film, while the polymer mid-block of the bq-PDMS strongly anchor into the grafted PDMS film by hydrophobic interactions. (ii) When given sufficient relaxation times under high tensile load, bq-PDMS molecules around the contact area perimeter are pulled out from the PDMS film, transferring to the mica surface. (iii) Bridging adhesion continues until the bq-PDMS molecules at the apex of the surface are pulled out from the PDMS film at $D_{Bridge} = D^{*}_{Bridge}$, a mica-PDMS separation distance near the fully extended length of bq-PDMS.

where $D_E > R_F$. Taking τ_R to be the sampling period between measurement points ($\tau_R^D = 0.5$ s for dynamic measurements and $\tau_R^Q = 30$ s for quasi-static measurements) and D_E to be the difference between the measured onset of attraction and the Au-PDMS film thickness ($D_E = D_A - D_0$), the Flory radius of the aggregate protrusions is estimated as 4.0 nm < R_F < 6.1 nm. This polymer-like behavior suggests that even longer-ranged attractive forces would be observed if the equilibration time is increased beyond 30 seconds; however, to observe a meaningful increase in the onset of attraction beyond the 30 second waiting time case, the waiting time must increase to experimentally-impractical intervals (on the order of 10 minutes), due to the exponential function of the exploration time. The timescale over which these aggregates fluctuate resembles the range for the "slow" characteristic relaxation times of whole micelles in solution, generally called τ_2. In surfactant micellar solutions, τ_2 corresponds to the timescale of the micellization-dissolution process—or the micelle

stability—and it generally falls in the range of hundreds of microseconds to tens of seconds for short aliphatic surfactants (in contrast to the much shorter lifetimes of the individual surfactant molecules in the micelles).[44,45] This rough analysis demonstrates that the 'fluctuating micelle' hypothesis is a viable possibility. After the capture event and collapse of the layer, the bq-PDMS headgroups are strongly attached to the mica, and a very strong adhesion is measured upon separating the surfaces, as discussed in the following section.

2.2. Asymmetric Interactions Between bq-PDMS and Mica Surfaces During Separation

The separation of bq-PDMS/mica surfaces leads to a very large adhesion force and exhibits highly rate-dependent interactions, similar to the approach interactions shown above. **Figure 3**A shows a comparison between a dynamic

separation (red points), and a quasi-static separation (blue points). In a dynamic separation, a tensile load is applied to the surfaces at a constant rate ($\dot{F}/R \approx 8.5$ mN m^{-1} s^{-1}); in a quasi-static separation, the tensile load is applied in increments ($F/R \approx 5$–15 mN m^{-1}) and the system is allowed to equilibrate for 30 s after each increase in tensile load (average $\dot{F}/R \approx 0.3$ mN m^{-1} s^{-1}). Additionally, under certain tensile loads during the quasi-static run, the surfaces were allowed to fully equilibrate for longer time periods (≈ 10–50 minutes), indicated by the blue squares during the quasi-static separation run (see Supporting Information). These two different modes of separating the surfaces allow for observation of differences in the rate-dependent polymer chain behavior between the surfaces as they are separated. The dynamic separation exhibits an extremely strong adhesion energy of $E_{ad} = -240$ mJ m^{-2}. This adhesion is dramatically smaller, $E_{ad} = -72$ mJ m^{-2}, when the separation is performed quasi-statically. Interestingly, when the surfaces are allowed to equilibrate under a strong tensile load, the surfaces slowly creep apart, observed as an increase in separation distance while the applied force remains constant (labeled as "constant force bridging", Figure 3A). At a tensile load of $E = -55$ mJ m^{-2}, the surfaces extend from $D = 7$ nm to $D = 10$ nm. Increasing the tensile load to $E = -62$ mJ m^{-2} causes the surfaces to extend further from $D = 10$ nm to $D = 11$ nm. Increasing the tensile load to $E = -68$ mJ m^{-2} leads to extension from $D = 11$ nm to $D = 12$ nm. Ultimately, when the negative tensile load reaches the measured adhesion energy, $E_{ad} = -72$ mJ m^{-2}, the surfaces bridge dramatically before the jump-out, from $D = 12$ nm to $D = 22$ nm. The average quasi-static adhesion energy measured over multiple experiments is $E_{avg} = -77 \pm 8$ mJ m^{-2}. The extension of the force curve before the jump-out indicates that the polymer chains of the bq-PDMS molecules relax and untangle from the Au-PDMS chains that are attached to the anchoring gold surface.

The characteristic "L" shape of the force curve during a quasi-static separation has been previously observed for separating tethered ligand-receptor bonds,[42] peeling polymers from a hydrophobic interface,[46] and specific interactions of tethered polymers with a target surface.[46,47] This kind of force-distance profile is observed when the specific endgroup-target surface attraction is stronger than the anchoring interaction.[42] In the present case, within the contact area between the bq-PDMS and mica surfaces, the bq-PDMS headgroups attach strongly and specifically to the mica surface, while the polymer mid-blocks anchor into the grafted Au-PDMS layer through hydrophobic interactions (Figure 3B.i). When the two surfaces are slowly separated from molecular contact, the bq-PDMS polymer chains are provided enough time to slowly rearrange, untangle, and extend out from the grafted Au-PDMS layer (Figure 3B.ii). Due to the surface curvature, bq-PDMS molecules around the perimeter of the given contact area are the first molecules to fully extend and are plucked from the Au-PDMS surface, breaking contact between the hydrophobic segments of the bq-PDMS and Au-PDMS chains. Bq-PDMS molecules around the contact area perimeter are continually extended and removed from the Au-PDMS surface, causing the contact area to shrink, until eventually only the chains at the apex bridge between the

two surfaces (Figure 3B.iii). The bridging molecules at the apex extend all the way to $D^{*}_{Bridge} = 15$ nm—nearly the fully extended length of the bq-PDMS molecules, $L_C \approx 20$ nm. For two curved surfaces, the force-law for the molecular pullout is independent of D,[42] and the force is therefore constant as D increases from D_0 to D^{*}_{Bridge}, at which point the rupture occurs. After the last bridging bq-PDMS molecule is plucked from the Au-PDMS, the two surfaces rapidly jump apart.

The strength of the specific Coulombic attraction between the bq-PDMS headgroup and the mica surface is stronger than the equilibrium hydrophobic interaction between the bq-PDMS and Au-PDMS chains, so bq-PDMS molecules are pulled out of the Au-PDMS film and transferred onto the mica surface. Material transfer of bq-PDMS onto the mica surface was confirmed by FECO and by a repeated force run at the same contact position, as shown in the Supporting Information (Figure S.2). The measured adhesion is thus effectively due to separation of the two PDMS interfaces (bq-PDMS and Au-PDMS), and the average adhesion energy $E_{avg} = -77 \pm 8$ mJ m^{-2} approaches the thermodynamically expected adhesion between two hydrophobic PDMS films or surfaces, $E_0 = -2\gamma_i = -88$ mJ m^{-2}, where $\gamma_i = 44$ mJ m^{-2} is the PDMS-water interfacial tension. E_{avg} is slightly less than E_0 due to the presence of cationic headgroups and excess surfactants near the hydrophobic failure interface. While the adhesion energy between extended hydrophobic surfaces decreases with moderate increases in temperature,[48] no significant change in the adhesion energy was measured over the small range of temperatures used in this study (22–26 °C).

Particularly noteworthy is the large difference in the adhesion values due to quasi-static and dynamic separations: $E_{ad} = -72$ mJ m^{-2} *vs* $E_{ad} = -240$ mJ m^{-2}, respectively. In the quasi-static case, the polymer chains re-arrange and reach preferred low-energy configurations, allowing the bq-PDMS molecules to be progressively pulled out of the Au-PDMS through a low-energy pathway. Thus, slow and quasi-static separations provide the lower bound and equilibrium adhesion energy between soft polymer surfaces. In contrast, during dynamic separations, the polymers do not have time to relax and rearrange, and the detachment or 'pull-off' between the bq-PDMS and Au-PDMS chains occurs simultaneously over the entire contact region, leading to energy dissipation in the entangled polymer film and much larger measured adhesion (see also Bell's theory on bond lifetimes).[49] To gain further physical insights into the proposed fluctuating aggregates and bridging forces, we also measured the forces between two bq-PDMS coated surfaces, to compare with the asymmetric bq-PDMS/mica interactions.

2.3. Symmetric Interaction Between bq-PDMS Interfaces

A thin PDMS film can also be supported on mica surfaces, using similar click chemistry with an amine-terminated silane monolayer on the mica surface (rather than the amine-terminated thiol monolayer used on gold).[48] A symmetric experiment between bq-PDMS layers was performed, in which a bq-PDMS layer supported on Au-PDMS interacts with a similar bq-PDMS layer supported on mica-PDMS.
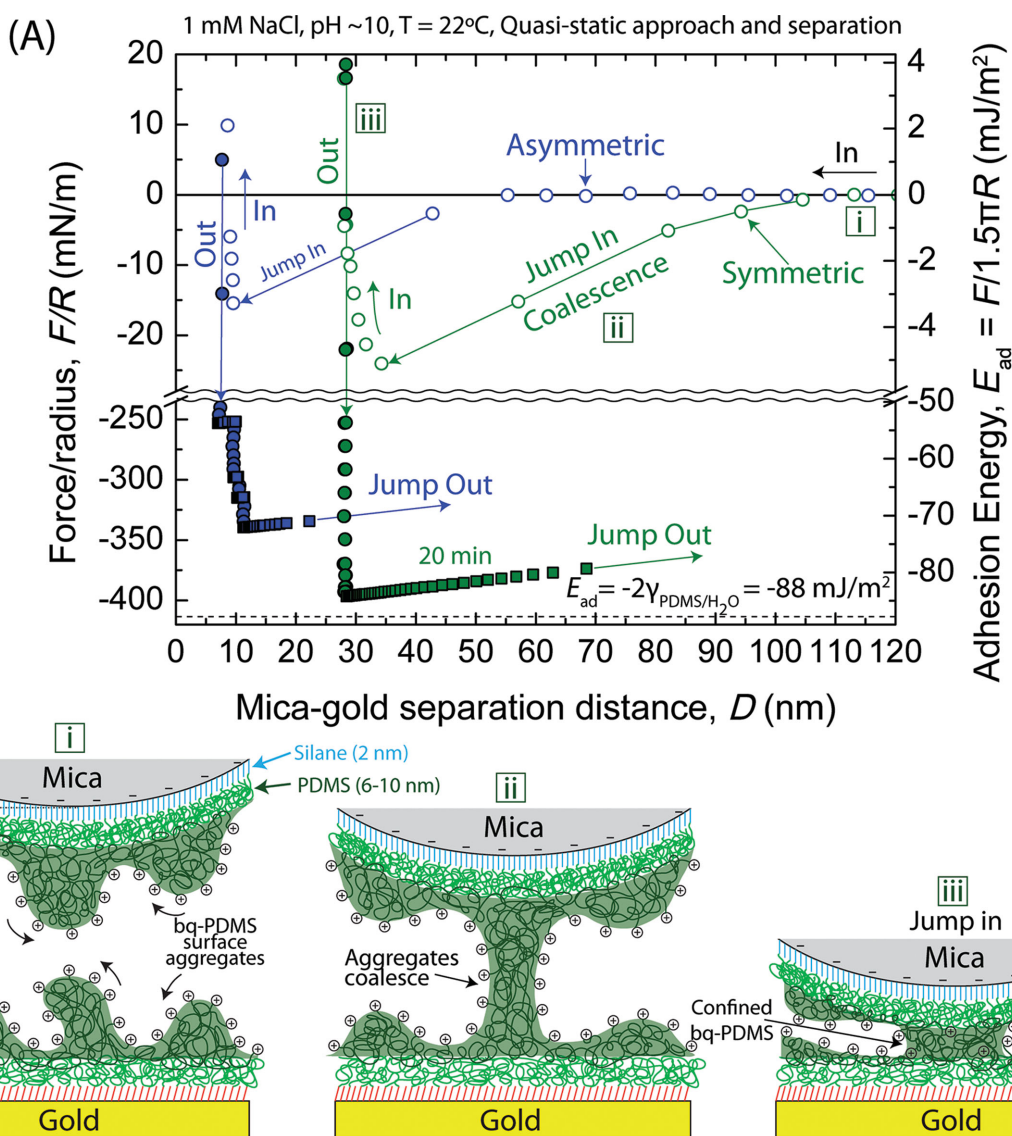
Figure 4. The forces between two symmetric bq-PDMS films. (A) Quasi-static force-distance measurements for the approach and separation of two symmetric bq-PDMS films (green circles/squares). Near the adhesive minimum, the system was allowed to equilibrate under a constant tensile load, and bridging adhesion was observed over 20 minutes (closed green squares). The asymmetric interaction between mica and one adsorbed bq-PDMS film on approach and separation is shown as blue circles/squares (same data as the quasi-static measurements shown in Figure 4, for comparison). (B) A schematic representation of the hypothesized interaction potential on approach of two symmetric bq-PDMS films. (i) The undulating bq-PDMS films approach one another. (ii) At large separation distances, the bq-PDMS aggregates coalesce and bridge the two surfaces. (iii) The coalesced bridge collapses, pulling the surfaces into a strong adhesive contact. Some bq-PDMS is confined between the grafted PDMS films.

Figure 4 shows a comparison of the asymmetric interaction of bq-PDMS and mica surfaces with the symmetric interaction of two bq-PDMS interfaces. The same data discussed above for the asymmetric quasi-static separation (Figure 3A, blue points) and its corresponding approach measurement are shown also in Figure 4 for comparison to the symmetric experiment. The symmetric experiment (Figure 4, green points) exhibits several qualitative similarities to the asymmetric experiment: during the approach, a very long-ranged attraction is observed, and during separation, the characteristic "L" shaped polymer-bridging force-distance profile is observed (filled green points). However, important differences between the symmetric and asymmetric experiments

are detected, which can help explain and confirm the proposed mechanisms discussed above.

The major difference between the symmetric and asymmetric experiments is the range of interaction, for both the approach and separation force-distance curves. During the approach in the asymmetric experiment, the attractive force onsets near $D = 49$ nm and jumps-in to a contact distance of $D_0 = 10$ nm, with an approximate range of interaction of 39 nm. The range of interaction increases for the symmetric system, with an attractive force onset near $D = 105$ nm, eventually jumping-in to a contact distance of $D = 28$ nm, corresponding to a range of interaction of about 77 nm. The range of interaction has therefore doubled for the symmetric

interaction compared to the asymmetric one. This is consistent with the protruding aggregates model, now adsorbed on both surfaces as shown in Figure 4B, approaching each other (Figure 4B.i), then encountering each other and coalescing (Figure 4B.ii), leading to the observed longer-ranged attraction. The large increase in the range of attraction further suggests that the protrusions are intrinsically dynamic and fluctuating structures; the nanostructures are not "activated" by the approach of another negatively charged surface, such as mica. No repulsive force was measured between the symmetric surfaces during a quasi-static approach, indicating that the attractive hydrophobic force between critically extended bq-PDMS aggregates overwhelms any repulsive electrostatic force between the similarly charged aggregates. A simple energy balance between the electrostatic, van der Waals, and hydrophobic pair potentials between two model nano-aggregates ($R \approx 4$ nm) indicates that these aggregates will coalesce even at moderate-to-high surface charge densities.

Interestingly, the attractive force leads to collapse of the protruding aggregates, although a significant amount of bq-PDMS appears to be trapped in the gap between the surfaces, as indicated by the hard-wall distance for the asymmetric ($D = 8$ nm) vs symmetric ($D = 28$ nm) cases (Figure 4B.iii). A naïve expectation would be that the hard-wall distance should double in this case; however, the hard-wall distance has increased by 3.5 times for the symmetric experiment. In the case of bq-PDMS approaching a bare mica surface, the bq-PDMS headgroups can spread on the mica surface, leading to a full collapse of the bq-PDMS layer. For two bq-PDMS surfaces, both surfaces already are fully saturated (if not oversaturated) with bq-PDMS and therefore cannot spread, and a significant amount is trapped between the surfaces, leading to the larger than expected hard-wall distance for the symmetric case. This result also suggests that the protruding aggregates are possibly formed due to an excess of bq-PDMS material at the PDMS thin film surface. Micron-sized lipid "worms" have previously been found to dynamically form and protrude at overpacked phospholipid bilayer-covered interfaces by fluorescence imaging,[50] however the proposed bq-PDMS nanostructures are too small to image with fluorescence, and too dynamic and soft to image with atomic force microscopy[51,52] (AFM images produced only smeared-out and featureless images of the bq-PDMS surface, Figure S3, Supporting Information).

The separation curve for two bq-PDMS surfaces also exhibits a larger range of interaction compared to the bq-PDMS/mica separation curve. The bridging distance increases from $D^*_{\text{Bridge}} = 15$ nm for the asymmetric case to $D^*_{\text{Bridge}} = 40$ nm for pulling apart two bq-PDMS surfaces. The dramatic increase in the polymer bridging distance indicates that bq-PDMS molecules, perhaps some in the form of bq-PDMS aggregates, extend between the two surfaces and lead to the measured bridging force. Only a single step-wise bridging event occurs for the symmetric separation in Figure 4A, as only one extended equilibration time was permitted past the bridging threshold load in this particular experiment. The average adhesion energy between two bq-PDMS coated surfaces $E_{\text{avg}} = -79 \pm 9$ mJ m^{-2} is slightly less than the expected thermodynamic adhesion for two PDMS interfaces,

$E_0 = -88$ mJ m^{-2}, similar to the adhesion between bq-PDMS and mica, further confirming that the strong adhesion (in both the asymmetric and symmetric cases) arises from the energy of cohesion between PDMS surfaces.

3. Conclusions

We have shown that long-chain bolaform surfactants self-assemble at hydrophobic interfaces and form more complicated and dynamic morphologies than previously reported for short-chain aliphatic surfactants. Short-chain aliphatic surfactants are known to adsorb to solid hydrophobic surfaces, form small structures (monolayers, hemicylinders, hemimicelles) similar in dimension to their bulk micelle size, and give rise to primarily electrostatic double layer forces when interacting with another surface in solution. By adsorbing a long-chain bolaform surfactant (bq-PDMS) onto a hydrophobic polymer brush film—drastically increasing the complexity of the system—we have found that dynamically fluctuating nanoscale surfactant aggregates form on the surface and persist for many hours. These bq-PDMS aggregates behave analogously to grafted polymer chains, as they fluctuate and explore their full configuration space. In measurements with the SFA, these aggregates induce an attractive force with an approaching mica surface as the aggregates contact the mica surface and the cationic surfactant headgroups bind to mica. The range of this attractive force (and the range of the abrupt jump in to adhesive contact) depends significantly on the rate of approach; decreasing the approach speed allows the aggregates to sample larger extended configurations, re-organize, and contact the mica surface at larger separation distances. The range of the attractive force and jump-in also increases with increasing temperature. When two similar surfaces of adsorbed bq-PDMS film approach in solution, the surface aggregates on opposite surfaces coalesce and give rise to a long-ranged bridging force.

These particular surface structures presumably exist only for specific combinations of surfactant geometries and surface types. Small changes to the surfactant molecule—such as changing the backbone composition, the backbone length, or the headgroup charge (changing the surfactant "packing factor")—or small changes to the surface structure—such as changing the surface hydrophobicity, degree of cross-linking, or polymer brush length—are all expected to affect the adsorbed surfactant structures and colloidal forces in complex ways. We are currently investigating this phenomenon with follow-up work.

The results presented in this study suggest that careful consideration should always be given to the rates at which measurements are performed at soft polymer interfaces. By varying the rate and method by which we separate a mica surface from the adsorbed bq-PDMS films, we find large differences in the separation mechanism and in the measured adhesion energy. When the separation is performed quickly, the polymer chains are not allowed enough time to relax and untangle, and consequently a massive—mostly dissipative—adhesion energy is measured. However, when the separation is performed slowly with sufficient waiting times, the

mica-bound bq-PDMS surfactants untangle and are pulled out from the underlying polymer layer, which manifests as slowly equilibrating molecular bridging force that extends nearly to the stretched length of the bq-PDMS molecules. This slow pull-out effect produces an adhesive energy that approaches the equilibrium adhesion energy between PDMS surfaces. These rate- and time-dependent effects should also arise when soft polymer surfaces, polymer-coated colloidal particles, or emulsions are sheared, mixed, or agitated, as these movements also involve two surfaces or particles approaching, and then separating, in a suspending liquid.

These cationic long-chain surfactants mediate remarkably strong adhesion between a polymer and a mineral surface, with adhesive forces that are significantly greater than those observed between hydrophobic and hydrophilic surfaces bridged by adhesive proteins.[24–26] The adhesive mechanisms displayed by these surfactants lend themselves well to applications such as binding lubricating films to anionic surfaces or securing polymer devices onto mineral or oxide films. The polymer mid-blocks of the surfactants entangle within a non- or partially-crosslinked polymer surface; the entangled polymer interface can dissipate energy during unloading or shearing events, leading to exceptionally large non-equilibrium adhesion energies. During separation of the mica and bq-PDMS surfaces, the specific Coulombic interactions between the quaternary ammonium surfactant headgroups and the mica surface are strong enough to shift the interface of failure to the hydrophobic PDMS-PDMS interface between the surfactant tails and the grafted polymer layer. This constitutes an important strategy for the design of robust adhesives in wet environments: whenever possible, shift the failure interface between the surfaces to a cohesive hydrophobic interface, as this results in an equilibrium adhesive energy that approaches a thermodynamic value of $E_{ad} = -2\gamma \approx -2(50 \text{ mJ m}^{-2}) \approx -100 \text{ mJ m}^{-2}$.

4. Experimental Section

Grafted PDMS Film Preparation: The full details of the Au-PDMS and mica-PDMS film preparation are described in our previous work.[14] To prepare Au-PDMS films for SFA measurements, cylindrical disks (area ≈ 1 cm²) of molecularly smooth gold are produced through a mica-templating technique. These clean gold surfaces are immersed in a 1 mM solution of 11-amino-1-undecanethiol hydrochloride (Sigma-Aldrich) for 2 hours and then rinsed with ethanol, forming an amine-functionalized self-assembled monolayer (SAM). The SAM surfaces are submerged and heated in neat monoglycidyl ether-terminated polydimethylsiloxane (MW = 5,000 g mol⁻¹, Sigma-Aldrich) at 130 °C for 1 hour. A click-chemistry reaction proceeds between the PDMS epoxide ring and the SAM amine group, to produce a covalently grafted PDMS film. Non-grafted PDMS is removed from the surface with cycles of rinsing and sonicating in toluene and ethanol.

In the symmetric experiment between two bq-PDMS surfaces, one mica-PDMS surface and one Au-PDMS surface were used instead of two Au-PDMS surfaces, because an insufficient amount of light transmits between two Au-PDMS surfaces and FECO is not observed. To prepare a mica-PDMS film,[51] a clean mica surface is treated with ozone for 20 minutes to activate the surface hydroxyl groups. The mica surface is amine-functionalized through immersion in a 1 vol% solution of (3-trimethoxysilylpropyl)diethylenetriamine (DETAS, Gelest Inc., Morrisville, PA) in methyl ethyl ketone (MEK, Sigma-Aldrich) for 2 hours. Next the surface is rinsed with ethanol, dried, immersed in monoglycidyl ether-terminated polydimethylsiloxane and then placed into a vacuum oven at 80 °C for 60 hours. The remaining preparation steps are exactly the same on mica-PDMS as they are on Au-PDMS.

Bq-PDMS Vesicle Preparation and Adsorption: Bq-PDMS (formally, α,ω-[diethylmethyl{isopropoxypropanol}ammonium chloride]-polydimethylsiloxane, MW = 4238 g mol⁻¹) was provided by the Proctor & Gamble Company (Cincinnati, Ohio). Bq-PDMS was mixed in hexylene glycol (≈ 6.4*10⁻⁷ moles bq-PDMS/L hexylene glycol) to form stable bq-PDMS vesicles. Au- or mica-PDMS surfaces were immersed in a small vial (≈2 mL) filled with the bq-PDMS/hexylene glycol mixture, and bq-PDMS vesicles were allowed to adsorb onto the surface for 1.5 h. Varying the adsorption time from 1–3.5 h did not alter the measured forces. Following the adsorption step, the reservoir of bq-PDMS/hexylene glycol surrounding the surface was replaced with a 1 mM NaCl pH ≈ 10 solution through a solvent exchange procedure. The small vial (2 mL), containing the surface and bq-PDMS/hexylene glycol solution, was submerged in a larger vial (≈30 mL) of 1 mM NaCl pH ≈ 10 solution and was gently mixed for 1 minute. The small vial—containing a bq-PDMS/hexylene glycol mixture diluted 15x with aqueous solution—was then removed from the larger vial. This dilution procedure was performed 10 times (using a fresh 1 mM NaCl solution during each dilution) to ensure that only negligible amounts of non-adsorbed bq-PDMS and hexylene glycol could exist in the reservoir surrounding the target surface. The bq-PDMS surface, resting in the small vial, was then transferred under solution into the SFA for force measurements. During the adsorption, dilution, and transfer process, the bq-PDMS surface was kept continually under solution; if the bq-PDMS surfaces were exposed to air at any point in the preparation, the subsequent force measurements would return non-reproducible results, and the long-ranged attractive forces to mica (attributed to the bq-PDMS nanostructures) were not observed. This result is not surprising, as exposure to air collapses the self-assembled bq-PDMS aggregates, and most likely washes a significant portion of bq-PDMS from the Au-PDMS surface with the receding air-water interface.

SFA: SFA measurements were performed with an SFA 2000 (manufactured by SurForce LLC., Santa Barbara, California). The SFA results presented here are representative of force measurements performed over more than 10 separate experimental setups. Prior to all SFA experiments, the SFA system was allowed to fully equilibrate at a given temperature, until no thermal or mechanical drift was observed.

Cryo-TEM: Cryo-TEM images were performed with a Tecnai TEM at Proctor & Gamble's facilities in Cincinnati, Ohio. Bq-PDMS/hexylene glycol vesicle mixtures (6.4 x 10⁻⁷ moles bq-PDMS/L hexylene glycol) were dispersed in water at a 1% v/v ratio. The introduction of the bq-PDMS vesicles into water did not alter the vesicle size, as confirmed with DLS. The samples were prepared for analysis by placing ≈2 µl of sample onto a lacey carbon grid, blotting away the excess and plunging the specimen rapidly into liquid ethane using a controlled environment vitrification system. The frozen samples were stored under liquid nitrogen until being

loaded into a Gatan model 626 cryo-stage. The specimens were then loaded into the TEM and imaged at 120 KV in low dose mode.

[1] B. D. Ratner, *Biomaterials science: an introduction to materials in medicine*, Academic press, Burlington, Massachusetts **2004**.

[2] D. F. Williams, *Biomaterials* **2008**, *29*(20), 2941–2953.

[3] F. Stapleton, S. Stretton, E. Papas, C. Skotnitsky, D. F. Sweeney, *Ocul. Surf.* **2006**, *4*(1), 24–43.

[4] A. Khademhosseini, R. Langer, J. Borenstein, J. P. Vacanti, *Proc. Natl. Acad. Sci. USA* **2006**, *103*(8), 2480–2487.

[5] J. Bongaerts, K. Fourtouni, J. Stokes, *Trib. Int.* **2007**, *40*(10), 1531–1542.

[6] A. Dyson, A. Wilson, In Paper 3: Film Thicknesses in Elastohydrodynamic Lubrication by Silicone Fluids, Proceedings of the Institution of Mechanical Engineers, *Conference Proceedings*, SAGE Publications Scheveningen, The Netherlands **1965**; pp 97–112.

[7] S. K. Sia, G. M. Whitesides, *Electrophoresis* **2003**, *24*(21), 3563–3576.

[8] J. Yu, S. Chary, S. Das, J. Tamelier, N. S. Pesika, K. L. Turner, J. N. Israelachvili, *Adv. Funct. Mater.* **2011**, *21*(16), 3010–3018.

[9] B. Murarash, Y. Itovich, M. Varenberg, *Soft Matter* **2011**, *7*(12), 5553–5557.

[10] J. Kim, Y. Gao, C. Hebebrand, E. Peirtsegaele, M. E. Helgeson, *Soft Matter* **2013**, *9*(29), 6897–6910.

[11] M. E. Helgeson, S. E. Moran, H. Z. An, P. S. Doyle, *Nat. Mater.* **2012**, *11*(4), 344–352.

[12] P. Somasundaran, S. C. Mehta, P. Purohit, *Adv. Colloid Interface Sci.* **2006**, *128*, 103–109.

[13] C. La Torre, B. Bhushan, *J. Cosmetic Sci.* **2005**, *57*(1), 37–56.

[14] S. H. Donaldson Jr., S. Das, M. A. Gebbie, M. Rapp, L. C. Jones, Y. Roiter, P. H. Koenig, Y. Gizaw, J. N. Israelachvili, *ACS Nano* **2013**, *7*(11), 10094–10104.

[15] C. Tian, Y. Shen, *Proc. Natl. Acad. Sci.* **2009**, *106*(36), 15148–15153.

[16] H. Mishra, S. Enami, R. J. Nielsen, L. A. Stewart, M. R. Hoffmann, W. A. Goddard, A. J. Colussi, *Proc. Natl. Acad. Sci.* **2012**, *109*(46), 18679–18683.

[17] A. Gray-Weale, J. K. Beattie, *Phys. Chem. Chem. Phys.* **2009**, *11*(46), 10994–11005.

[18] P. Creux, J. Lachaise, A. Graciaa, J. K. Beattie, A. M. Djerdjev, *J. Phys. Chem. B* **2009**, *113*(43), 14146–14150.

[19] G. Fontani, R. Gaspari, N. D. Spencer, D. Passerone, R. Crockett, *Langmuir* **2013**, *29*(15), 4760–4771.

[20] S. Lee, N. D. Spencer, *Trib. Int.* **2006**, *38*(11), 922–930.

[21] J.-F. Argillier, M. Tirrell, *Theor. chim. acta* **1992**, *82*(5), 343–350.

[22] B. Liberelle, S. Giasson, *Langmuir* **2008**, *24*(4), 1550–1559.

[23] U. Raviv, S. Giasson, N. Kampf, J.-F. Gohy, R. Jérôme, J. Klein, *Langmuir* **2008**, *24*(16), 8678–8687.

[24] J. Yu, Y. Kan, M. Rapp, E. Danner, W. Wei, S. Das, D. R. Miller, Y. Chen, J. H. Waite, J. N. Israelachvili, *Proc. Natl. Acad. Sci.* **2013**, *110*(39), 15680–15685.

[25] H. Lee, B. P. Lee, P. B. Messersmith, *Nature* **2007**, *448*(7151), 338–341.

[26] Q. Lu, E. Danner, J. H. Waite, J. N. Israelachvili, H. Zeng, D. S. Hwang, *J. R. Soc. Interface* **2013**, *10*(79), 20120759.

[27] G. Mehta, M. J. Kiel, J. W. Lee, N. Kotov, J. J. Linderman, S. Takayama, *Adv. Funct. Mater.* **2007**, *17*(15), 2701–2709.

[28] J. N. Israelachvili, *Intermolecular and surface forces: revised*, 3rd ed. Academic press Burlington, Massachusetts **2011**.

[29] E. J. Wanless, W. A. Ducker, *J. Phys. Chem.* **1996**, *100*(8), 3207–3214.

[30] W. A. Ducker, L. M. Grant, *J. Phys. Chem.* **1996**, *100*(28), 11507–11511.

[31] J.-F. Liu, W. A. Ducker, *J. Phys. Chem. B* **1999**, *103*(40), 8558–8567.

[32] L. M. Grant, F. Tiberg, W. A. Ducker, *J. Phys. Chem. B* **1998**, *102*(22), 4288–4294.

[33] F. Tiberg, J. Brinck, L. Grant, *Curr. Opin. Colloid Interface Sci.* **1999**, *4*(6), 411–419.

[34] R. A. Johnson, R. Nagarajan, *Colloids Surf. A: Physicochem. Eng. Asp.* **2000**, *167*(1), 31–46.

[35] S. Manne, J. Cleveland, H. Gaub, G. Stucky, P. Hansma, *Langmuir* **1994**, *10*(12), 4409–4413.

[36] J. Israelachvili, Y. Min, M. Akbulut, A. Alig, G. Carver, W. Greene, K. Kristiansen, E. Meyer, N. Pesika, K. Rosenberg, *Rep. Progr. Phys.* **2010**, *73*(3), 036601.

[37] J. Israelachvili, *J. Colloid Interface Sci.* **1973**, *44*(2), 259–272.

[38] M. Ruths, J. N. Israelachvili, H. J. Ploehn, *Macromolecules* **1997**, *30*(11), 3329–3339.

[39] Y. L. Chen, S. Chen, C. Frank, J. Israelachvili, *J. Colloid Interface Sci.* **1992**, *153*(1), 244–265.

[40] P. Claesson, R. G. Horn, R. Pashley, *J. Colloid Interface Sci.* **1984**, *100*(1), 250–263.

[41] P. G. de Gennes, *Scaling Concepts in Polymer Physics*. Cornell University Press Ithaca, New York **1979**.

[42] J. Y. Wong, T. L. Kuhl, J. N. Israelachvili, N. Mullah, S. Zalipsky, *Science* **1997**, *275*(5301), 820–822.

[43] B. H. Zimm, *J. Chem. Phys.* **1956**, *24*(2), 269–278.

[44] E. Aniansson, S. Wall, M. Almgren, H. Hoffmann, I. Kielmann, W. Ulbricht, R. Zana, J. Lang, C. Tondre, *J. Phys. Chem.* **1976**, *80*(9), 905–922.

[45] A. Patist, T. Axelberd, D. O. Shah, *J. Colloid Interface Sci.* **1998**, *208*(1), 259–265.

[46] M. Valtiner, S. H. Donaldson Jr., M. A. Gebbie, J. N. Israelachvili, *J. Am. Chem. Soc.* **2012**, *134*(3), 1746–1753.

[47] S. H. Donaldson Jr., M. Valtiner, M. A. Gebbie, J. Haradad, J. N. Israelachvili, *Soft Matter* **2013**, *9*(21), 5231–5238.

[48] S. H. Donaldson Jr., A. Royne, K. Kristiansen, M. V. Rapp, S. Das, M. A. Gebbie, D. W. Lee, M. Valtiner, J. N. Israelachvili, *Langmuir* **2014**, DOI: 10.1021/la-2014-02115g.R1

[49] G. I. Bell, *Science* **1978**, *200* (4342), 618–627.

[50] K. Weirich, *Phd thesis,* University of California, Santa Barbara **2012**

[51] S. O'shea, M. Welland, T. Rayment, *Langmuir* **1993**, *9*(7), 1826–1835.

[52] H. Huang, S. E. Rankin, L. S. Penn, R. P. Quirk, T. H. Cheong, *Langmuir* **2004**, *20*(14), 5770–5775.